Climate Dynamics (2024) 62:4063–4079
https://doi.org/10.1007/s00382-024-07117-1

ORIGINAL ARTICLE

On the impact of net-zero forcing Q-flux change

Kai-Uwe Eiselt[1] · **Rune Grand Graversen**[1,2]

Received: 12 September 2023 / Accepted: 11 January 2024 / Published online: 22 February 2024

Abstract
Numerical climate model simulations suggest that global warming is enhanced or hampered by the *spatial pattern* of the warming itself. This phenomenon is known as the "pattern effect" and has in recent years become the most promising explanation for the change over time of climate sensitivity in climate models. Under historical global warming, different patterns of surface-temperature change have emerged, notably a yet unexplained cooling in the Southern Ocean and the East Pacific. Historical climate model simulations notoriously fail to reproduce this cooling, which may contribute to the deviation of the simulated global-mean warming from the observed record. Here we qualitatively investigate the potential impact of historical and other surface-temperature pattern changes by changing the ocean heat transport convergence (Q-flux) in a slab-ocean model. The Q-flux changes are always implemented such that in the global mean they impose no net forcing. Consistent with earlier studies we find that the impact of a negative Q-flux change in the Southern Ocean has a stronger effect than in other regions because of a feedback loop between sea-surface temperatures (SSTs) and clouds in the Southern Ocean and the stably stratified regions in the tropics. The SST-cloud feedback loop facilitates the expansion of the Antarctic sea ice, indeed taking the model into a Snowball-Earth state. The intensity of this effect is found to be model dependent, especially due to differences in the cloud parametrisation. In experiments with deactivated sea ice the impact of the negative Q-flux change is much weaker.

Keywords Climate sensitivity · Feedback · Pattern effect · Climate modeling · Ocean heat transport

1 Introduction

Global warming may be enhanced or hampered due to a change in warming patterns between regions. This process is known as the "pattern effect" (Stevens et al. 2016) and was discovered in numerical global climate model (GCM) simulations (Andrews et al. 2012, 2015). It has in recent years garnered prominence in climate change research. The mechanism of the pattern effect works as follows: Surface warming patterns evolve over time to favour or disfavour regions of different atmospheric stability, giving rise to feedback processes that enhance or hamper cooling. Thus, the change in local warming patterns induces the global "cooling efficiency" to be reduced or increased over time (e.g., Andrews et al. 2012, 2015; Andrews and Webb 2018; Mauritsen 2016; Zhou et al. 2016, 2017; Ceppi and Gregory 2017; Dong et al. 2019, 2020). In most GCMs a CO_2 -induced surface warming shifts over time to regions which are characterised by relatively strong atmospheric stability, inhibiting cooling due to lapse-rate and cloud feedbacks (e.g., Andrews et al. 2015; Dong et al. 2020).

The efficiency with which the Earth is cooling in response to a forcing-induced warming is called the climate feedback. Employing the forcing F (e.g., due to an increase in the CO_2 -concentration) and the climate feedback parameter λ, the climate system is often represented by the simple linear relation:

$$\Delta N = F + \lambda \Delta T_s, \tag{1}$$

where ΔN is the change in the top-of-the-atmosphere (TOA) radiative balance, and ΔT_s is the change of the surface-air temperature (SAT). This framework is typically used to derive the so-called equilibrium climate sensitivity (ECS) from global climate models (GCMs), which is possibly

✉ Kai-Uwe Eiselt
kai-uwe.eiselt@uit.no

Rune Grand Graversen
rune.graversen@uit.no

[1] Department of Physics and Technology, University of Tromsø, Tromsø, Norway

[2] Norwegian Meteorological Institute, Tromsø, Norway

the most widely used single-number metric to describe the response of the climate system to a forcing. The ECS is usually defined as the global-mean SAT (GSAT) response to a doubling of the CO_2-concentration in the atmosphere and may be derived from Eq. 1 by assuming a new equilibrium condition ($\Delta N = 0$):

$$\mathrm{ECS} = -\frac{F_{2x}}{\lambda}, \tag{2}$$

where F_{2x} corresponds to the forcing due to the doubled CO_2 -concentration.

In the framework defined by Eq. 1, the changing global cooling efficiency over time implies a changing climate feedback parameter and thus, according to Eq. 2, a changing climate sensitivity over time. This time-dependence of climate sensitivity was discovered long ago (Murphy 1995; Senior and Mitchell 2000; Boer and Yu 2003; Gregory et al. 2004), but due to the lack of coordinated GCM experiments different conjectures were put forward and no general theory was formulated (see e.g., Eiselt and Graversen 2022, for a brief literature overview). Over the last ten years, from investigation of the coordinated experiments of the Coupled Model Intercomparison Project (CMIP) phases 5 (Taylor et al. 2009) and 6 (Eyring et al. 2016) as well as targeted individual model studies and comparisons with observations, the pattern effect finally emerged as a reasonable explanation for an important part of the time dependence of climate sensitivity (Andrews et al. 2012, 2015; Andrews and Webb 2018; Zhou et al. 2016, 2017; Dong et al. 2019, 2020)

Several specific geographical regions have been highlighted in the literature as either exhibiting abnormal historical warming changes, or as having a significant impact on climate feedback. These regions include the Indo-Pacific Warm Pool (IPWP), which has warmed comparatively strongly over the historical period and has been found to significantly influence climate feedback (Mauritsen 2016; Zhou et al. 2016, 2017; Dong et al. 2019, 2020). This is because the IPWP exhibits strong convective activity, meaning that a surface warming is quickly distributed to higher atmospheric layers. Here the warming is readily spread horizontally over large areas and the associated internal energy is efficiently radiated into space. Thus, a relatively strong warming in the IPWP implies a relatively strong negative climate feedback (Dong et al. 2019).

Another region is the Eastern Pacific (EP), which in spite of global warming has exhibited a cooling trend over the last forty years (e.g., Wills et al. 2022). Some studies also indicate this latter region's possible importance for climate feedback changes, especially in more recent climate models, mainly due to its effect on short-wave cloud feedback from low-cloud-cover changes (Ceppi and Gregory 2017; Andrews and Webb 2018; Dong et al. 2020). Clouds have both warming and cooling impacts on the climate: Warming because they impede long-wave radiation from escaping to space and cooling because they reflect incoming solar radiation. Since low clouds are relatively warm, their impact on the long-wave radiation and thus their warming effect is small. Conversely, low clouds have a strong cooling effect because they are optically dense, meaning they reflect a large fraction of the solar radiation back to space (e.g., Wallace and Hobbs 2006). Tropical marine low cloud cover has been found to be strongly controlled by sea-surface temperature (SST) and atmospheric stability (e.g., Klein et al. 2017). Hence, the surface warming in the EP may be important in driving the cloud feedback. The short-wave cloud feedback tends to dominate the uncertainty in the total feedback across GCMs, also in the latest generation (e.g., Zelinka et al. 2020), implying the EP as potentially important for climate feedback change. Notably, it is unclear why despite global warming the EP has cooled. Competing hypotheses exist such as that the cooling is a result of internal variability but it has also been proposed that the cooling is a forced dynamical ocean (e.g., the so-called "ocean thermostat"; Clement et al. 1996; Luo et al. 2017; Lee et al. 2022) and/or atmosphere (e.g., the so-called "iris effect"; Lindzen and Choi 2021; Mauritsen and Stevens 2015; Lee et al. 2022) response to CO_2-concentrations changes.

An additional region is the Southern Ocean, which, in parts, has exhibited a similar cooling trend as the EP over the same period and has been shown to have a potentially large impact on climate feedback and sensitivity through local and teleconnection effects. That is, similar to the EP, SSTs and stability influence the local cloud feedback, but it has also been found that a warming/cooling in the Southern Ocean affects the EP, influencing the cloud feedback there through SST and stability changes, as described above (Hwang et al. 2017; Lin et al. 2021; Kim et al. 2022; Dong et al. 2022; Kang et al. 2023). As for the EP, it is unclear why the Southern Ocean has historically cooled. Suggested explanations include internal variability (Zhang et al. 2019) and fresh-water input from Antarctic ice-sheet melt Dong et al. (2022). Notably, due to the teleconnection and feedbacks described in Kim et al. (2022), Dong et al. (2022), and Kang et al. (2023), the EP cooling is potentially driven by the Southern Ocean cooling.

Finally, the North Atlantic is the focus of many studies as it is strongly influenced by the Atlantic meridional overturning circulation (AMOC), impacting the local surface warming (He et al. 2017; Lin et al. 2019; Bellomo et al. 2021; Eiselt and Graversen 2023). Indeed, a lack of warming in the North Atlantic (the so-called North Atlantic Warming Hole, NAWH) is found in many climate models in CO_2-forcing experiments and is thought to be connected to a decline of the AMOC (e.g., Bellomo et al. 2021). Several studies indicate the influence of a decline of the AMOC on climate

sensitivity, mainly due to impacts on sea ice, surface-albedo, and lapse-rate feedback (He et al. 2017; Lin et al. 2019; Mitevski et al. 2023; Eiselt and Graversen 2023).

To test the impact of the warming/cooling patterns, we perform slab-ocean model (SOM) experiments where energy is redistributed horizontally across the Earth's surface by changing the ocean heat-flux convergence (the so-called Q-flux). Specific warming/cooling patterns may be induced in a SOM with a positive Q-flux change (i.e., heat-flux *con*vergence) leading to a local warming and vice versa. The experiments are motivated by the observed changes in surface-warming patterns described above as well as by projected changes under CO_2-forcing. We repeat the AMOC-mimicking experiment described by Eiselt and Graversen (2023), where positive and negative Q-flux changes are implemented in the tropical and the North Atlantic, respectively. This experiment is based on an order-of-magnitude estimation of the Q-flux change induced by differences in AMOC change between fully-coupled abrupt CO_2-quadrupling experiments. However, in contrast to Eiselt and Graversen (2023), the CO_2 remains at pre-industrial levels (284.7 ppm), to isolate the effect of the Q-flux change. Motivated by the observed historical cooling in the EP and the relative warming in the IPWP, we perform an experiment with negative and positive Q-flux change in these regions, respectively. Similarly, in order to investigate the historical cooling in the Southern Ocean, experiments are run with negative Q-flux change in parts of and the whole Southern Ocean and positive Q-flux change in parts of or the whole tropics. In contrast to the AMOC-mimicking experiment no quantitative analysis is performed to relate the Q-flux changes to results from fully-coupled model experiments for these regions. However, in order to maintain comparability, the Q-flux changes integrated over the individual regions are equivalent to those in the AMOC-mimicking experiment. We note that the cooling induced by the negative Q-flux changes in the EP and the Southern Ocean is much stronger than is observed historically. To investigate the impact of the Q-flux change magnitude we run additional experiments with Q-flux changes in the Southern Ocean that are similar to historical changes of Southern Ocean heat uptake (e.g. Huguenin et al. 2022). Importantly, in order to not to introduce a global net forcing from the Q-flux changes, the integrated net Q-flux change in all experiments is zero.

2 Models and experiments

2.1 CESM and the slab-ocean model

The Community Earth System Model version 2.1.3 (CESM2; Danabasoglu et al. (2020)) in the slab-ocean model (SOM) configuration is applied. A SOM is similar to a fully-coupled GCM in that it couples several dynamical model components of the climate system. However, the difference is that in a SOM the dynamical ocean component is replaced by an isothermal mixed-layer ocean with a spatially varying mixed-layer depth (MLD) and a seasonally and spatially varying lateral ocean heat transport, called Q-flux. The Q-flux is derived from a fully-coupled GCM control simulation under equilibrium conditions from the MLD, the SSTs, and the ocean heat uptake of the dynamical ocean model component (Bitz et al. 2012).

In a SOM, the SST tendency $\frac{\partial \mathrm{SST}}{\partial t}$ is determined as follows (Bitz et al. 2012):

$$\frac{\partial \mathrm{SST}}{\partial t} = \frac{F_{net} + Q_{flx}}{\rho_0 c_p h}, \tag{3}$$

where F_{net} comprises the fluxes from the atmosphere to the ocean and/or sea ice, Q_{flx} is the ocean heat transport convergence (hereafter Q-flux), ρ_0 is the density of seawater, c_p the ocean heat capacity, and h is the MLD. Note that F_{net} is determined dynamically, while the Q-flux is prescribed. Hence, SST patterns may be changed in a SOM by changing the Q-flux.

To test the sensitivity of our results to model version, we additionally employ an earlier version of the same model (CESM1; Hurrell et al. 2013), as well as a version of CESM2 with a changed cloud parametrisation (CESM2-Z22; Zhu et al. 2022). The cloud parametrisation of CESM2-Z22 was explicitly calibrated to exhibit greater skill in simulating the Last Glacial Maximum (LGM) climate than CESM2. Notably, also CESM1 simulates the LGM climate more realistically than does CESM2 (Zhu et al. 2021). The differences in cloud parametrisations have been implicated as the main reason for the differences in ECS between the three model versions (CESM2: 5-6 K; CESM1: 3-4 K, CESM2-Z22: ~4 K; Gettelman et al. 2019; Bacmeister et al. 2020; Bjordal et al. 2020; Zhu et al. 2022). For detailed model descriptions as well as a discussion of the differences between models see Text S1 in the online supplemental material.

2.2 Experiment design

Building on Eiselt and Graversen (2023), we conduct several experiments with a Q-flux change in a particular region, always compensated by an opposite-sign Q-flux change in another region to ensure net-zero global forcing. Hence, the imposed climate response is solely due to regional energy redistribution and not to a global forcing. Following Eiselt and Graversen (2023), the Q-flux change is ramped up linearly over the first year and then held constant throughout the experiment. The CO_2-concentration as well as all other forcing agents are left at their pre-industrial levels, in order to isolate the effect of the pattern changes. To calculate

anomalies, the climatology of a 30-year control experiment with unchanged Q-flux was subtracted. Our three main experiments are listed in the following. See Table 1 for a summary of all experiments conducted for this study.

dQ-AMOC Here, negative and positive Q-flux changes are implemented in the North Atlantic ($50-80°N, 285-25°W$) and the tropical Atlantic ($15°S-15°N, 285-25°W$), respectively (Fig. S1 in the online supplemental material). This experiment is equivalent to the "dQ" experiment in Eiselt and Graversen (2023), although without $4xCO_2$. The purpose of the experiment is to mimic the decline of the AMOC, as simulated by several CMIP5 and CMIP6 members in response to $4xCO_2$ (see the appendix in Eiselt and Graversen (2023) for the derivation of the Q-flux change induced by the AMOC change).

dQ-EP-WP A negative Q-flux change is implemented in the EP ($0-30°S, 255-280°W$) and the compensating positive Q-flux change in the IPWP ($15°S-15°N, 60-180°W$; Fig. S2). The experiment may be thought of as mimicking the historical cooling of the EP and the comparatively fast warming of the IPWP, although the SST changes induced by the Q-flux change are much larger than those historically observed.

dQ-SA-TA Several experiments have been conducted with negative Q-flux change in parts of or the whole Southern Ocean and a compensating positive Q-flux change in parts of or the whole tropics. These experiments may be thought of as mimicking the historical cooling and/or increased ocean heat uptake of the Southern Ocean (e.g., Huguenin et al. 2022). Here, we focus on the example of an experiment that is similar to dQ-AMOC, only "flipped" at the equator (dQ-SA-TA) with the region in the South Atlantic being $50-70°S$ and $305-30°W$, and in the tropical Atlantic 15 S − 15°N and $285-25°W$ (Fig. S3). As in dQ-EP-WP, the local cooling induced by the Q-flux change is much larger than the historical trends in the Southern Ocean. Further experiments with smaller and potentially more realistic Q-flux changes are conducted (Table 1).

Further experiments To test the linearity of the response to the pattern and CO_2-concentration changes, the three main experiments described above are rerun with quadrupled CO_2-concentration. In addition, a simulation is performed where only CO_2 is quadrupled and no Q-flux change is implemented. To test the potential impact of sea ice on the linearity of the response, the dQ-SA-TA experiment is rerun again with deactivated sea ice. Similar to Rugenstein et al. (2016), we deactivate the sea ice by setting the freezing temperature of salt water to a very low value (for a detailed description see Text S2 in the online supplemental material).

Many studies have the weakness of investigating the impact of Q-flux changes in only one model (e.g., Liu et al. 2018a, b, 2020; Lin et al. 2021; Singh et al. 2022; Dong et al. 2022; Eiselt and Graversen 2023). Our focus here is also on one model (CESM2), but to allow for at least some model diversity we additionally perform the main experiments with a previous version of the same model (CESM1). In addition, to investigate the potential impact of the cloud parametrisation on the pattern effect, we perform the main experiments also with CESM2-Z22 which is equivalent to CESM2, except for adjustments to the cloud microphysics parametrisation scheme (see Sect. 2.1 and Text S1 in the online supplemental material).

3 Methods

3.1 Radiative kernel method

The radiative kernel method (Soden et al. 2008; Shell et al. 2008) can be used to decompose the climate model response into individual physical feedbacks and is based on two main assumptions: (1) The radiative response ΔN of the climate system at TOA can be expressed as a function of independent climate variables:

$$\Delta N = F + (\lambda_{Pl} + \lambda_{LR} + \lambda_{SA} + \lambda_{WV} + \lambda_{C})\Delta T_s, \tag{4}$$

where λ_{Pl}, λ_{LR}, λ_{SA}, λ_{WV}, and λ_{C} are the feedback parameters due to changes in Planck radiation, temperature lapse rate (LR), surface albedo (SA), water-vapour (WV) mixing ratio,

Table 1 Summary of Q-flux change experiments. The columns with "Snowball" only concern CESM2

Name	Negative δQ region	Positive δQ region	δQ in Wm^{-2}	Snowball $1xCO_2$	Snowball $4xCO_2$
dQ-AMOC	50–80° N; 285–25° W	15° S-15° N; 285–25° W	– 51, 26	No	No
dQ-EP-WP	0–30° S; 255–280° W	15° S-15° N; 60–180° W	– 50, 11	Yes	No
dQ-SA-TA	50–70° S; 305–30° W	15° S-15° N; 285–25° W	– 49, 26	Yes	Yes
dQ-SEP-TA	50–70° S; 200–280° W	15° S-15° N; 285–25° W	– 51, 26	Yes	Yes
dQ-SEP-EP	50–70° S; 200–280° W	0–30° S; 250–280° W	– 51, 49	Yes	No
dQ-SO-T-3Wm^{-2}	50–70° S	15° S-15° N	– 3, 1.2	Yes	(N/A)
dQ-SO-T-2Wm^{-2}	50–70° S	15° S-15° N	– 2, 0.8	No	(N/A)

and cloud properties, respectively. (2) The dependence of the TOA radiative flux on a change in one of the climate variables is linear. Radiative kernels are derived by changing one of these climate variables in the radiation code of a climate model. Since radiation codes are well tested and similar across models (Soden et al. 2008), one set of radiative kernels can be used to derive the radiative fluxes from different climate models and experiments. Under the assumptions introduced above the kernel can then be multiplied on the change of the variable in question in an experiment with another climate model, hereby deriving the TOA radiative flux change due to the change in this variable. The feedback parameter λ_i for a climate variable i may be obtained by regressing the kernel-derived TOA radiative flux change due to the change in i on the GSAT change (Gregory et al. 2004; Block and Mauritsen 2013). A more detailed description of the kernel method is presented in Text S3 in the online supplemental material.

Here we use the set of radiative kernels provided by Shell et al. (2008). For details on the choice of radiative kernels see Eiselt and Graversen (2022).

4 Results

In the following we discuss the results of the Q-flux change experiments described in Sect. 2.2. We mainly focus on CESM2, but in Sect. 4.3 results are compared across CESM1, CESM2, and CESM2-Z22.

4.1 Response to different Q-flux pattern changes

In this section we compare the response of CESM2 to the three different net-zero-forcing Q-flux change experiments dQ-AMOC, dQ-EP-WP, and dQ-SA-TA. The comparison is conducted mainly in terms of the SAT change and individual feedbacks.

dQ-AMOC The mimicked change of the AMOC leads to a decline of the GSAT of about 3 K after 50 years of simulation (Fig. 1a). The effect is strongest in the Northern Hemisphere (NH) extra-tropics (-8 K), while there is much less of an impact in the tropics (-2 K) and the Southern Hemisphere (SH) extra-tropics (-1 K). Figure 2a shows the individual climate feedbacks and their evolution over time. Initially, the LR and cloud feedback are largest, followed by the SA and WV feedbacks. However, because the impact of the Q-flux change in this experiment is comparatively weak on the global level, especially the cloud feedback exhibits strong uncertainty in the first few years. In a zonal-mean decomposition (Figs. S4 and S5 in the online supplemental material), it is revealed that the LR and SA effects concentrate in the NH polar region (>50° N), while the effect of the cloud feedback is spread over most of the NH extra-tropics, with some additional effect in the deep tropics, due to partly compensating long-wave and short-wave cloud effects. The positive LR and SA feedbacks appear to be related to the Arctic sea ice, which quickly expands over the first decade of the simulation (Fig. 1d). The increased sea-ice area leads to more reflection of sunlight, causing a negative SA radiative flux, inducing a positive (i.e., cooling) feedback. Moreover, the sea ice insulates the atmosphere from the ocean. In the polar regions the ocean acts as a heat source for the atmosphere. Thus, an increase in sea-ice cover induces a cooling

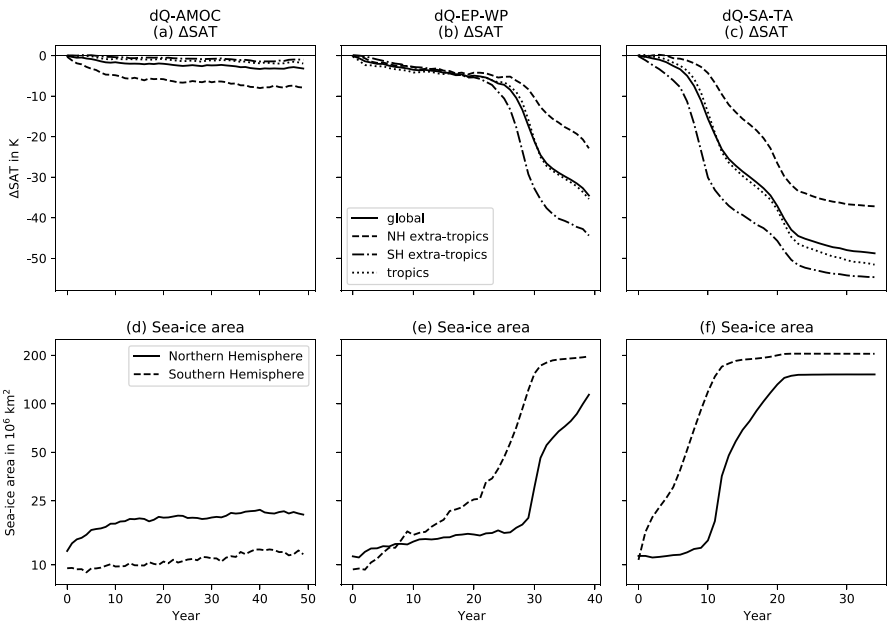

Fig. 1 Surface-air temperature response (ΔSAT) and sea-ice area for (**a**, **d**) dQ-AMOC, (**b**, **e**) dQ-EP-WP, and (**c**, **f**) dQ-SA-TA. For the ΔSAT are shown (solid) global means, (dotted) tropical means (30° N-30° S), and extra-tropical means over the (dashed) Northern Hemisphere (>30° N) and (dash-dotted) Southern Hemisphere (>30° S). Northern Hemisphere and Southern Hemisphere sea-ice areas are depicted as solid and dashed lines, respectively in panels (**d**–**f**). The sea-ice area is shown on a logarithmic scale

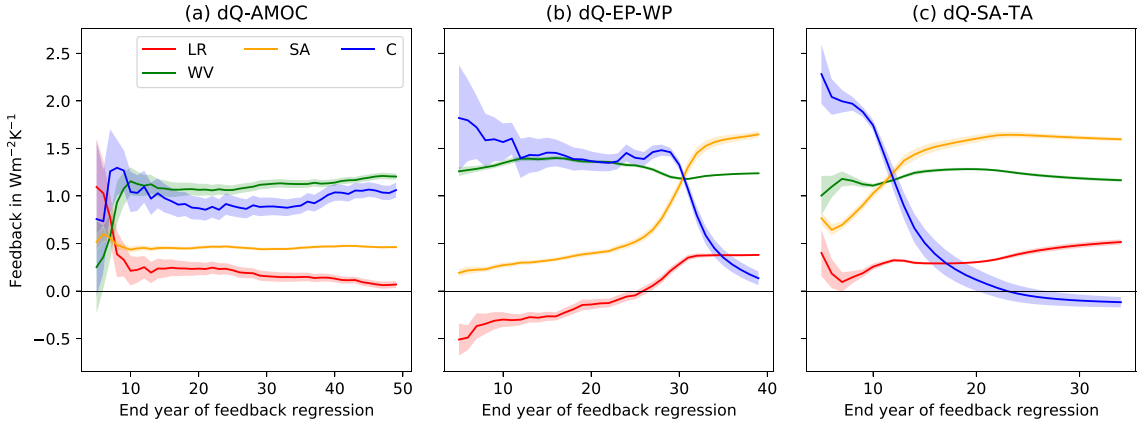

Fig. 2 Feedback time series in **a** dQ-AMOC, **b** dQ-EP-WP, and **c** dQ-SA-TA as simulated by CESM2. Shown are the (red) lapse-rate, (green) water-vapour (WV), (orange) surface-albedo (SA), and (blue) cloud (C) feedbacks. The feedbacks are calculated by regressing the radiative kernel derived top-of-the-atmosphere (TOA) radiative fluxes on the global-mean surface-air temperature (Gregory et al. 2004; Block and Mauritsen 2013). The starting year of the regression is always year 1 while the end year is continuously incremented from year 5 to the final year. The radiative kernels provided by Shell et al. (2008) were used. Note the different x-axis scales

influence at the surface, increasing atmospheric stability, hereby leading to a positive LR feedback. A positive LR feedback also results without the generation of new sea ice because of the relative surface cooling from the negative North Atlantic Q-flux change. With the saturation of the growth of the Arctic sea ice (Fig. 1d), the LR and SA feedbacks decline (Fig. 2a).

dQ-EP-WP The response of the GSAT in dQ-EP-WP is much stronger than in dQ-AMOC. The GSAT decreases by about 7 K at year 25 of the simulation, after which the decline rapidly accelerates, taking the model into a Snowball Earth state (Fig. 1b,e). The main impact of the Q-flux change is on the cloud and WV feedbacks, with a minor contribution from the SA feedback and a negative contribution from the LR feedback (Fig. 2b). Note that dQ-EP-WP is different from dQ-AMOC and dQ-SA-TA (see below) since it exhibits a negative LR feedback while the other two experiments exhibit a positive LR feedback (Fig. 2). This is associated with the spatial structure of the LR feedback, being generally negative at low and positive at high latitudes, due to convection at low and strong atmospheric stability at high latitudes (Manabe and Wetherald 1975). In dQ-EP-WP the impact of the Q-flux change is a strong surface cooling of the tropics, affecting the convective regions and cooling the higher atmospheric layers. This leads to a reduction of the outgoing long-wave radiation, hereby inducing a globally negative (i.e., warming) LR feedback. However, due to the persistent general cooling the sea ice grows continually (Fig. 1e), amplifying the surface cooling at the high latitudes, which, due to the stability in these regions is not readily vertically distributed. Hence, the surface cools more strongly than the upper atmospheric layers, eventually giving rise to a globally positive LR feedback. In contrast to dQ-EP-WP, in the other experiments the sea-ice effect is active immediately from the start of the simulation, because the Q-flux change impact is concentrated at the high latitudes. Thus, the LR feedback is positive throughout the simulation in these experiments. The differences between the experiments highlight the importance of the latitudinal aspects of the pattern effect in influencing global climate feedback, especially regarding the LR feedback (see also Lin et al. 2019; Singh et al. 2022; Mitevski et al. 2023; Eiselt and Graversen 2023).

The strongly positive cloud feedback is concentrated in the tropics (Figs. S4 and S5), and particularly in the East Pacific (EP; Fig. S6). The EP is a relatively stably stratified region and the Q-flux-change-induced surface cooling in dQ-EP-WP further increases the stability. The SSTs and the estimated inversion strength (EIS; a measure for atmospheric stability; Wood and Bretherton 2006) are strong cloud controlling factors, especially influencing tropical low cloud (Klein et al. 2017). Note again that clouds generally have two climate feedback effects: A cooling effect due to increased reflection of incoming solar radiation and a warming effect by blocking thermal radiation from exiting to space. Low clouds mainly cause the former effect as they are optically thick and thus exhibit a high albedo, while they are also relatively warm, implying a weak impact on the outgoing thermal radiation (e.g., Wallace and Hobbs 2006). The effect on short-wave radiation is especially strong for liquid clouds, since liquid cloud droplets are smaller and more densely packed than cloud ice crystals, causing a higher cloud optical depth and thus albedo (Stephens 1978). Hence, the surface cooling and the accompanying increase in EIS in the EP induce increased local low-cloud cover, reflecting more of the incoming sunlight (Figs. S6 and S7), hereby amplifying the local surface cooling. The intense surface cooling

in the EP is advected westward across the central tropical Pacific (see Fig. S8b for the climatological winds), affecting EIS, low-cloud cover, and short-wave cloud radiative flux (CRF_{SW}) to the west of the Q-flux anomaly.

As compared to the EP, the positive Q-flux change implemented in the IPWP does not as strongly impact the SSTs there. Indeed, because of the strong convective characteristics of this region, heat is quickly spread vertically. In the free troposphere, it is readily distributed horizontally, in fact potentially contributing to the increasing EIS in the EP (e.g., Zhou et al. 2016, 2017; Mauritsen 2016; Andrews and Webb 2018; Dong et al. 2019). Energy associated with the heating in the free troposphere is also radiated to space more readily than is energy at the surface, hereby contributing to the global cooling.

The continued cooling in the tropics also impacts other regions (Fig. 1b), and in the Southern Ocean the cooling induces an expansion of the Antarctic sea ice (Fig. 1e). Through the SA feedback, this contributes further to the global cooling (Fig. 2b), eventually leading to an acceleration of the sea-ice expansion, driving the transition to the Snowball-Earth state (Fig. 1e). This transition proceeds similarly in the dQ-SA-TA experiment and is described in more detail below.

dQ-SA-TA The strongest response to the Q-flux change is found in the dQ-SA-TA experiment. The initial decline of the GSAT is similar to the dQ-EP-WP experiment, with the strongest feedback again being due to clouds (Fig. 2c). However, the pattern of the cloud feedback is different from that in the dQ-EP-WP experiment, by being spread over the SH subtropics and middle latitudes (Figs. S4 and S5). In addition a much stronger initial SA feedback due to the Antarctic sea-ice growth is encountered (Figs. 1f and 2c), which is induced by the negative Q-flux change in the South Atlantic. As the Antarctic sea ice expands, the SA feedback increases, while the cloud feedback declines, as clouds dissolve over the expanding ice (Figs. 2c and 3).

Considering regional radiative fluxes, initially there is a weak but extensive negative CRF_{SW} over the Southern Indian Ocean as well as a stronger negative CRF_{SW} over the Southern subtropical Atlantic (Fig. 3a). This appears to be due to the strong surface cooling in the South Atlantic induced by the Q-flux change and amplified by local sea-ice growth, which is quickly advected via climatological winds along the African and Australian coasts over the subtropical Atlantic and Indian Ocean (Fig. S8b). We note that the Southeast Pacific is initially (i.e., in the first about 5 years) not as strongly impacted as the other mentioned regions and exhibits relatively less cooling and only a small negative CRF_{SW}. This may be associated with the Antarctic sea ice exhibiting its smallest northward extent in the Southeast Pacific until about year 7 (Fig. 3c). From year 6 and onward, both the tropical Atlantic and Indian Ocean show increasingly negative CRF_{SW}, and from year 8 a similar effect is seen in the EP. This is consistent with the northern boundary of the Antarctic sea ice being situated at a similar latitude (circa 45° S) across the whole Southern Ocean at year 8 (Fig. 3d). The process in the EP is similar to that described for the tropical Atlantic and Indian Ocean: The cooling of the South Atlantic due to the negative Q-flux change and local feedbacks (SA, LR, cloud) is advected around Antarctica by climatological winds (Fig. S8b). Successively, this leads to an expansion of the sea ice also in the Southeast Pacific, which, again facilitated by local feedbacks, accelerates the cooling there. Through climatological winds along the coast of South America (Fig. S8b), this cooling impacts the EP region, locally inducing lower SSTs, causing an increase of EP stability. As mentioned above, tropical marine low clouds in stable regions are sensitive to SST and stability changes (e.g., Klein and Hartmann 1993; Wood and Bretherton 2006; Klein et al. 2017). The decrease of the SST and the increase of the stability lead to more low-cloud cover, reflecting the incoming solar radiation. A further SST cooling initiates a positive SST-cloud feedback loop: lower SSTs, more low cloud, less insolation, lower SSTs, more low cloud, etc. (Hwang et al. 2017; Kim et al. 2022; Dong et al. 2022; Kang et al. 2023). Over years 7 to 11 the tropical CRF_{SW} becomes increasingly negative, leading to the accelerated decline of the GSAT, and continuously causing the Antarctic sea ice to advance more equatorward (Fig. 3c–f). Finally, the cooled tropical regions together with the winds advecting along the west coasts of the continents facilitate the quick expansion of the Antarctic sea ice, leading to almost full coverage of the Southern Hemisphere by year 12 of the simulation (not shown).

As mentioned above, several dQ-SO-T-type experiments were conducted (see Table 1). The response of these experiments follows a similar trajectory as described for dQ-SA-TA. That is, implementing a negative Q-flux change in the Southeast Pacific with the positive Q-flux change being either in the tropical Atlantic (dQ-SEP-TA) or the tropical East Pacific (dQ-SEP-EP) causes an almost equivalent transition to a Snowball Earth as dQ-SA-TA (not shown). In another experiment where the negative Q-flux change is spread over the whole Southern Ocean and the positive Q-flux change over the whole tropics (dQ-SO-T-3Wm^{-2}), the response is linear and weak for over 30 years, after which an abrupt shift occurs, taking the model into a Snowball Earth. This shift appears to be driven by the SST-cloud feedback loop, especially in the East Pacific, as explained above (Figs. S9 and S10). Notably, in the latter experiment the Q-flux change in the individual regions is only about 1/4 of the Q-flux change in dQ-SA-TA. We report that in a further experiment (dQ-SO-T-2Wm^{-2}) with -2 Wm^{-2} Q-flux change over the whole Southern Ocean and a compensating positive change over the whole tropics, no Snowball Earth transition

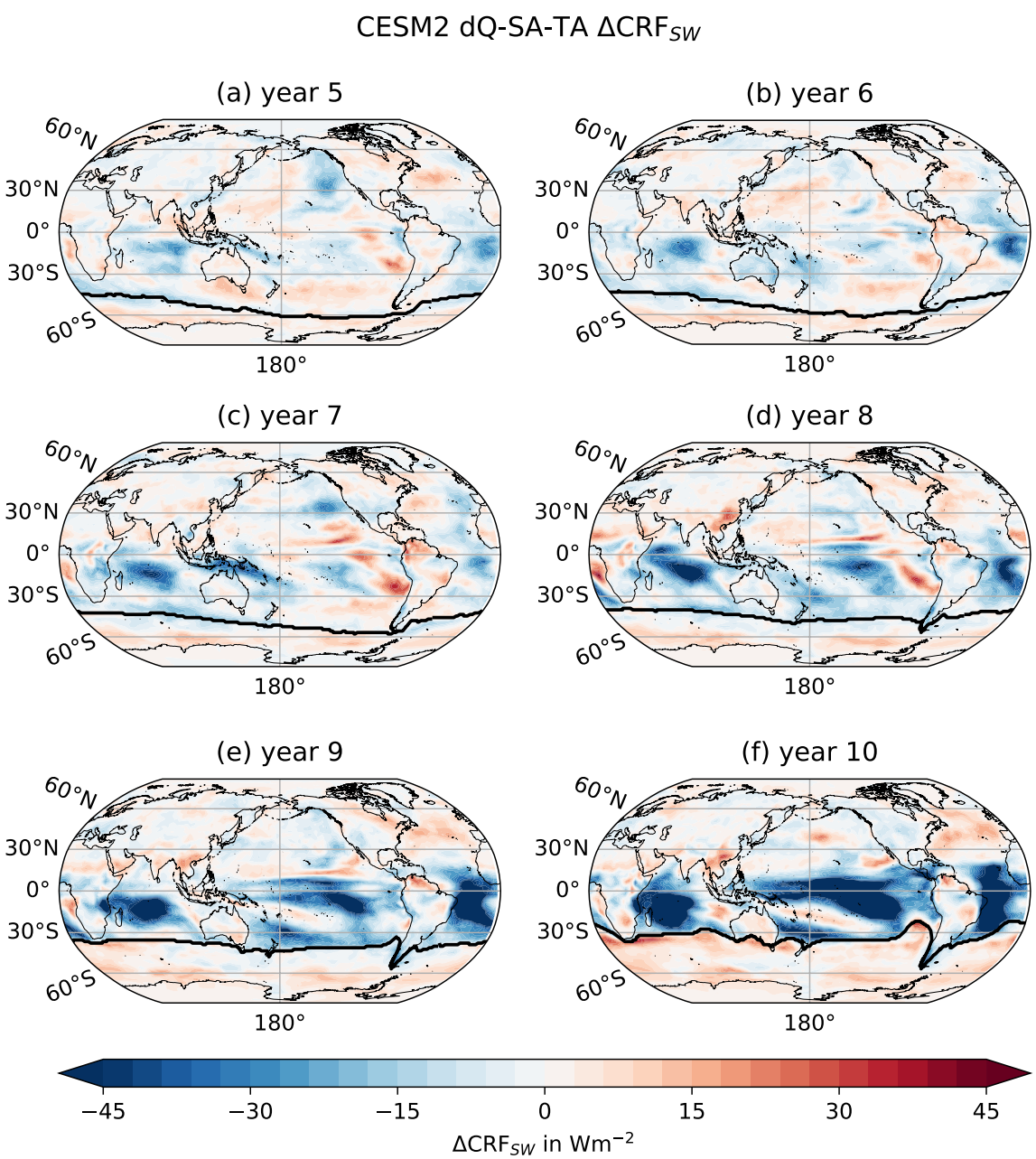

Fig. 3 Maps of annual means of the short-wave cloud radiative flux change (ΔCRF_{SW}) for years 5 to 10 of the dQ-SA-TA experiment as simulated by CESM2. The black line indicates the annual mean Antarctic sea-ice extent

is instigated. Remarkably, it is generally only when the cooling SST-cloud feedback loop in the EP is initiated that the model rapidly intensifies the negative CRF_{SW} and accelerates the sea-ice expansion facilitating the transition to a Snowball Earth state (see especially dQ-SO-T-3Wm^{-2}; Figs. S9 and S10).

Earlier studies investigating the impact of Q-flux changes in aquaplanet (e.g., Rose et al. 2014; Kang and Xie 2014) and real-world topography (e.g. Rugenstein et al. 2016; Liu et al. 2018a) configurations have found a larger impact of extra-tropical than of tropical Q-flux changes. This is generally attributed to a mostly local positive short-wave cloud feedback induced by the extra-tropical Q-flux changes, strengthening the warming/cooling of the Q-flux change. Conversely, in the tropics Q-flux changes tend to be locally balanced at TOA, thus having a smaller effect. It appears from our results that not only the meridional structure of the Q-flux changes is important, but also the regional structure, and that the NH and the SH have different impacts. Indeed, a cooling

Q-flux change has a much stronger effect when concentrated in the EP in contrast to being spread over the whole tropics, due to the strong link to low cloud cover in this region. Thus, similar to Q-flux changes in the extra-tropics, in the EP they induce a local positive feedback. Conversely, Q-flux changes in the North Atlantic only have a small impact on clouds, and their total climate impact is hence less than the changes of the Q-flux in the EP or the Southern Ocean.

Our results point to the importance of the Southern Ocean and are in line with earlier studies employing mostly older models in both similar (e.g., Lin et al. 2021; Dong et al. 2022) and different experimental set-ups (e.g., Hwang et al. 2017; Kim et al. 2022; Kang et al. 2023). Consistent with these earlier studies, Q-flux changes in the Southern Ocean are found to induce cloud feedbacks in the tropics, thus inducing not only local (as in Rose et al. 2014; Kang and Xie 2014) but also remote effects. As these remote effects result from real-world topography (i.e., deflection of climatological winds at the western mountain ranges of the SH continents), they would not be present in aquaplanet simulations. Notably, in experiments with older models the role of the so-called wind-evaporation-SST (WES) feedback (Xie and Philander 1994) has at least a similar impact as compared to the short-wave cloud feedback (e.g., Hwang et al. 2017; Kim et al. 2022). However, Kang et al. (2023) employing the more recent CESM2 find that the short-wave cloud feedback dominates, supporting our focus on this feedback.

As a final note, we want to emphasise that in contrast to most of the above-discussed earlier studies in our experiments no net-forcing is introduced. Thus, the climate-system response results solely from a *redistribution* of energy.

4.2 (Non-)Linearity of responses to Q-flux change and CO_2-forcing

Three different experiments are employed to test the linearity of the response to the Q-flux change and the CO_2-forcing (which induces the Q-flux change at least for dQ-AMOC). These include the Q-flux change experiments (dQ), the CO_2 experiment ($4xCO_2$), and the combined Q-flux-change and CO_2-forcing experiment (dQ&4x). To investigate linearity, we add up the responses of the dQ and $4xCO_2$ experiments (hereafter referred to as dQ+4x) and compare with the dQ&4x experiment. If the responses to dQ and $4xCO_2$ add linearly, dQ&4x and dQ+4x should yield similar results. dQ+4x and dQ&4x are compared for our three main experimental set-ups dQ-AMOC, dQ-EP-WP, and dQ-SA-TA.

As shown in Fig. 4, the GSAT response in all three set-ups is initially linear, i.e., dQ+4x and dQ&4x exhibit only small differences of $|\Delta| < 1$ K. In dQ-AMOC this difference is largest in the NH (~ -2.5 K), growing slightly throughout the 50-year simulation. This small non-linearity in the GSAT response appears to be driven by differences in sea-ice development giving rise to differences in SA and LR fluxes (Fig. S11a): In both the $4xCO_2$ and the dQ&4x experiments the Arctic sea-ice cover quickly declines, remaining constant after about 15 and 25 years, respectively (Fig. 5c). Conversely, in the dQ-AMOC experiment at $1xCO_2$, the Arctic sea ice quickly grows (Fig. 1d). The growth decelerates over time, but it continues at least until year 40. In dQ+4x the sea-ice growth in dQ-AMOC compensates the loss in $4xCO_2$ more than in the combined dQ&4x experiment. Thus, in dQ&4x more sea ice is lost than in dQ+4x, engendering the above-mentioned SA and LR feedbacks, driving the deviation from a linear response to dQ-AMOC and $4xCO_2$. A smaller but over time growing contribution to the non-linearity

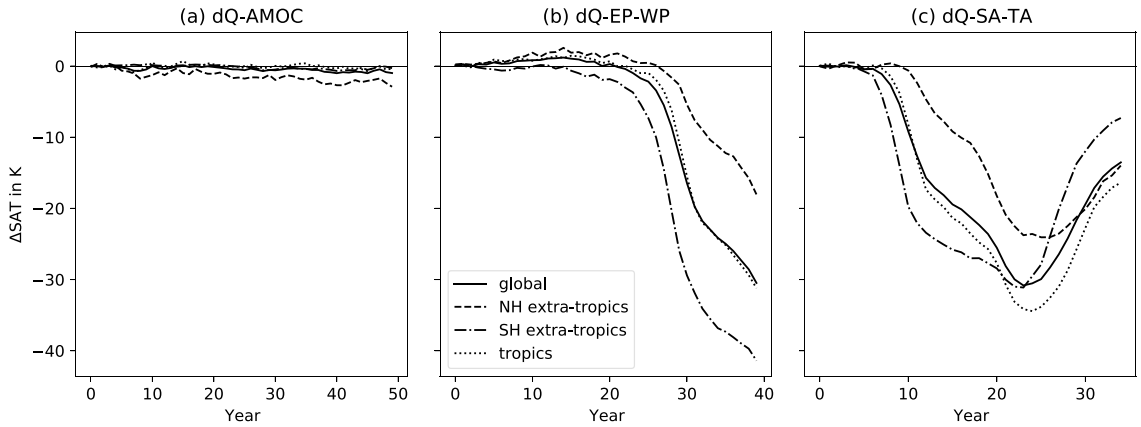

Fig. 4 Differences in surface-air temperature change (ΔSAT) between dQ+4x and dQ&4x (dQ+4x minus dQ&4x) for **a** dQ-AMOC, **b** dQ-EP-WP, and **c** dQ-SA-TA. Shown are (solid) global means, (dotted) tropical means (30° N-30° S), and extra-tropical means over the (dashed) Northern Hemisphere (NH; >30° N) and (dash-dotted) Southern Hemisphere (SH; >30° S). Note the different x-axis scales

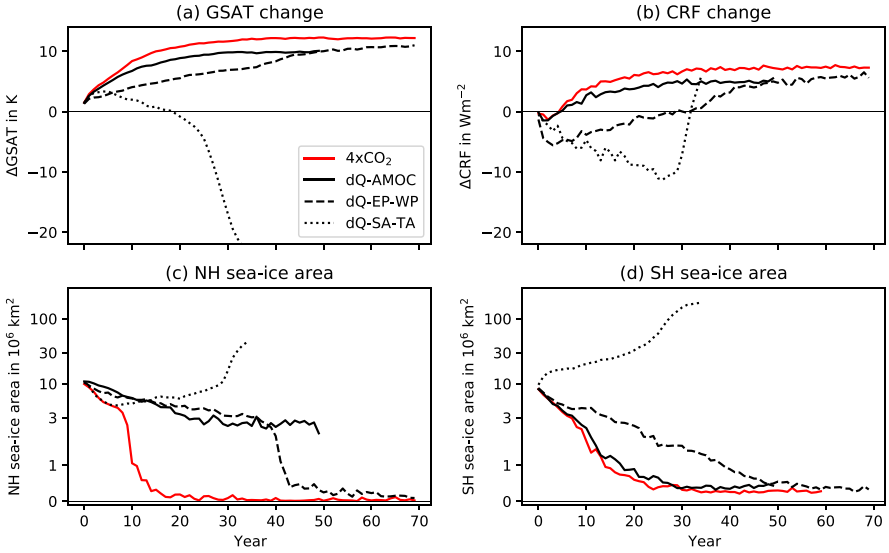

Fig. 5 Global means of **a** surface-air temperature change (ΔGSAT) and **b** cloud radiative flux (ΔCRF), as well as **c** Northern Hemisphere (NH) sea-ice area, and **d** Southern Hemisphere (SH) sea-ice area for the CESM2 experiments (solid red) 4xCO_2, (solid black) dQ-AMOC, (dashed) dQ-EP-WP, and (dotted) dQ-SA-TA. All dQ experiments were run with quadrupled CO_2-concentration. The sea-ice area is shown on a logarithmic scale

comes from the Antarctic sea ice: dQ&4x and 4xCO_2 exhibit almost equivalent Antarctic sea-ice decline, i.e., dQ-AMOC has little effect on Antarctic sea ice under concomitant 4xCO_2 (Fig. 5d). However, in dQ-AMOC with 1xCO_2, after some time the Antarctic sea ice starts growing slowly, triggering LR and SA feedbacks similar to the Arctic sea ice, thus contributing to the GSAT difference between dQ+4x and dQ&4x.

In contrast to dQ-AMOC, dQ-EP-WP and dQ-SA-TA quickly exhibit strongly non-linear responses (Fig. 4b,c). These are related to the Antarctic sea-ice expansion in dQ-EP-WP and dQ-SA-TA under 1xCO_2, which is driven by the cloud-SST feedback loop in the Southern Ocean and the tropics as explained in Sect. 4.1. While in the dQ-SA-TA set-up eventually the Antarctic sea ice expands and a Snowball Earth state is obtained also under 4xCO_2-forcing (Fig. 5), this is delayed compared to the 1xCO_2 simulation: In dQ&4x the rapid sea-ice expansion starts only after year 25, while under 1xCO_2 this occurs already around year 8 (Fig. 1c, f). Thus, in the dQ-SA-TA set-up in terms of GSAT the dQ+4x minus dQ&4x difference quickly becomes strongly negative, expressing the non-linearity of the response. However, after the Antarctic sea-ice expansion accelerates also in dQ&4x (Fig. 5d) the difference between dQ+4x and dQ&4x declines and starts approaching zero. Thus, while the *transient* response to dQ-SA-TA and 4xCO_2 is strongly non-linear, the *equilibrium* response may be linear, although the simulations conducted here are not long enough to confirm this.

dQ-EP-WP is different from dQ-SA-TA because under 4xCO_2 it does not enter a Snowball Earth state (Fig. 5). Hence, the difference in terms of GSAT between dQ+4x and dQ&4x becomes strongly negative (similar to dQ-SA-TA) when the Antarctic sea ice starts its accelerated expansion in dQ-EP-WP under 1xCO_2, but, unlike in dQ-SA-TA, the difference never recovers. Hence, in dQ-EP-WP *both* the transient and the equilibrium response to dQ and 4xCO_2 may be described as non-linear.

The difference of the response to dQ-EP-WP and dQ-SA-TA under 1xCO_2 and 4xCO_2 highlights the importance of the location of the Q-flux change and of the impact of the sea ice. Similar to dQ-AMOC, it is the effect of the high-latitude Q-flux change in dQ-SA-TA which leads to the maintenance of the sea-ice cover despite the quadrupled CO_2-concentration. Conversely, even though the negative Q-flux changes in dQ-EP-WP and dQ-SA-TA are of similar magnitude, in dQ-EP-WP they do not impact the sea ice *directly*. Under 4xCO_2 the impact of the CO_2-forcing on the sea ice, facilitated particularly by strongly positive extra-tropical CRF_{SW} (Fig. S12), is thus stronger than the Q-flux impact, causing sea-ice retreat and hence additional warming SA and cloud radiative fluxes (Fig. S13b), prohibiting the transition to a Snowball Earth. In contrast, in dQ-SA-TA the Q-flux change directly impacts the Antarctic sea ice more than the CO_2 -forcing, causing its local expansion and the accompanying cooling SA, LR, and cloud radiative fluxes (Fig. S13c). As explained above, the effect eventually spreads to the tropics, similar to the 1xCO_2 dQ-SA-TA experiment, causing the expansion of the Antarctic sea ice and the transition to the Snowball-Earth state.

To further investigate the effect of the sea ice, we rerun the dQ-SA-TA experiments (under 1x and 4xCO_2) and the 4xCO_2 experiment, but with no sea ice present. In this set-up, dQ+4x shows 2 K more warming than dQ&4x, thus exhibiting a much more linear response than the experiments with sea ice (Fig. 6). The difference is primarily caused by the cloud feedback (Fig. 7), especially over the Southern Ocean (Fig. S14) and the EP (not shown). The CO_2-forcing and the Q-flux change have competing impacts on the cloud radiative fluxes, especially over the Southern Ocean: The CO_2-forcing induces a positive CRF, while the Q-flux change

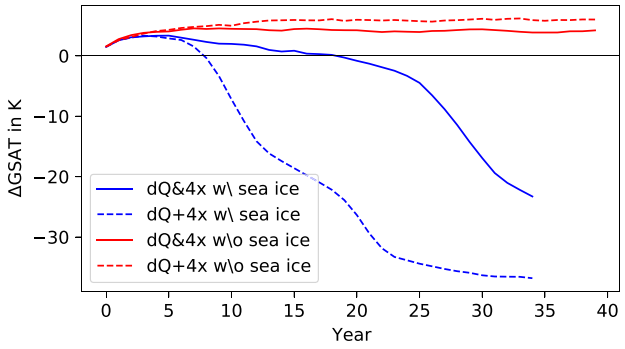

Fig. 6 Global-mean surface-air temperature change (ΔGSAT) in the dQ-SA-TA experiment (blue) with sea ice and (red) without sea ice for (solid) dQ&4x and (dashed) dQ+4x

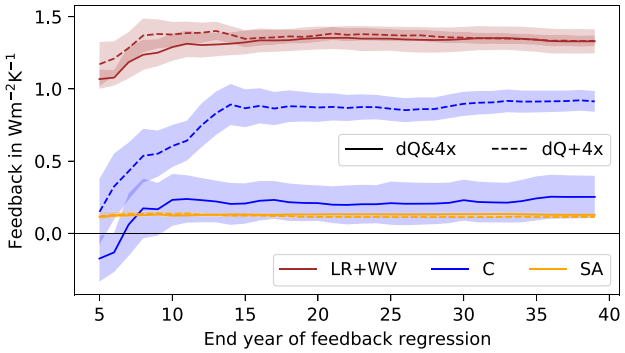

Fig. 7 As Fig. 2 but for dQ-SA-TA under (solid) dQ&4x and (dashed) dQ+4x. Note that here the lapse-rate and water-vapour feedbacks are summed (they are generally anti-correlated; Po-Chedley et al. 2018) to increase the clarity of the figure

induces a negative CRF. A self-reinforcing SST-cloud feedback loop is initiated, warming in 4xCO_2 and cooling in dQ, as described in Sect. 4.1. Without sea ice a stronger feedback loop is induced in 4xCO_2 than in dQ, leading to a positive total CRF in dQ+4x. In dQ&4x the feedback loop is muted because of the compensating impact of the Q-flux change and the CO_2-forcing, implying a smaller CRF. Thus, the sum of the cloud effects in the separate dQ and 4xCO_2 experiments is larger than the effect in the combined experiment, giving rise to the difference in cloud feedback seen in Fig. 7.

4.3 Comparing different model versions

Here our aim is to investigate the dependence of the impact of Q-flux changes on model version. To this end, we rerun our three main experiments (see Sect. 2.2) with CESM1, i.e., the previous version of CESM2, as well as with CESM2-Z22, which is structurally equivalent to CESM2 except for the cloud parametrisation (Zhu et al. 2022, for details see Text S1 in the online supplemental material).

The GSAT responses to dQ-AMOC and dQ-SA-TA are qualitatively similar in all three models, i.e., a moderate cooling and a transition to a Snowball Earth state, respectively (Fig. 8). Conversely, there is a large difference in dQ-EP-WP in CESM2 compared with CESM1 and CESM2-Z22. That is, CESM2 cools much quicker than the other two models, and transitions to a Snowball Earth state, whereas CESM1 and CESM2-Z22 only exhibit a moderate cooling, similar to their response in dQ-AMOC (see Fig. S15 for the sea-ice area).

Considering the radiative fluxes derived from the kernel method, the differences in GSAT response between the models appear to be explained by differences in the short-wave cloud response. CESM2 generally exhibits the strongest negative CRF_{SW} of the three models, especially in dQ-EP-WP and dQ-SA-TA (Fig. S16). Notably, the WV radiative flux is also strongly negative but the intensification of the CRF_{SW} precedes that of the WV flux, and we thus suggest that the

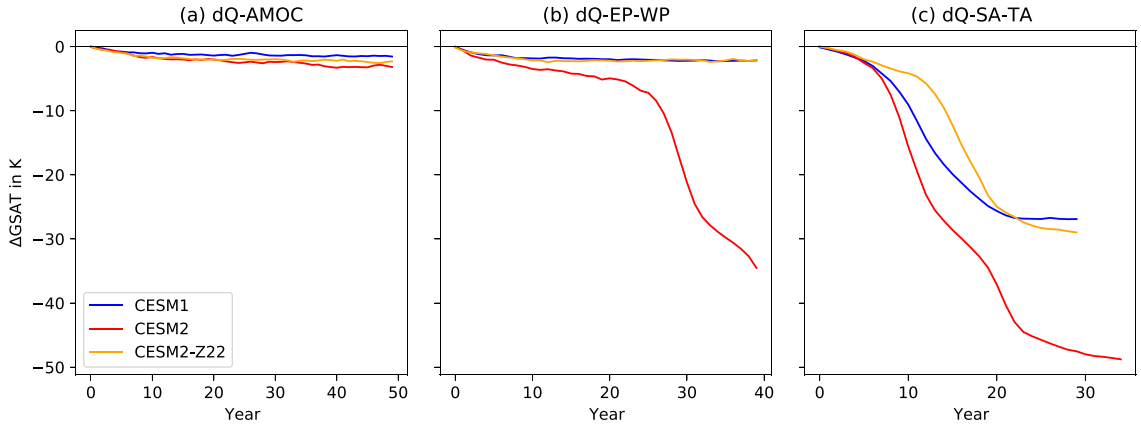

Fig. 8 Comparison of (blue) CESM1, (red) CESM2, and (orange) CESM2-Z22 in terms of global-mean surface-air temperature change (Δ GSAT) for cases **a** dQ-AMOC, **b** dQ-EP-WP, and **c** dQ-SA-TA. Note the different x-axis scales

WV flux may be viewed as a response to the temperature change which is mainly initiated by the CRF_{SW}.

The above-discussed differences in model response to the Q-flux changes may be related to several differences in model characteristics between the three model versions. First, it should be noted that the base-state Q-flux and the mixed-layer depth (MLD) in CESM1 are different from CESM2 and CESM2-Z22 (Fig. S17 and S18, respectively). Regions of large base-state Q-flux may be less impacted by the same Q-flux change as regions with small base-state Q-flux, since the Q-flux change would be *relatively* smaller. However, generally the annual-mean Q-flux in CESM1 and CESM2 appears similar in the regions of Q-flux change considered in this study (Fig. S17c). The influence of the MLD on the impact of the Q-flux on SSTs is described by Eq. 3: The larger the MLD, the smaller the impact of a given Q-flux change, meaning that the MLD effectively acts as a kind of thermal inertia. Regarding dQ-AMOC, the area-weighted MLD in the North Atlantic region of negative Q-flux change is somewhat lower in CESM2 than in CESM1 (178 m compared to 201 m), potentially facilitating the faster cooling and regional sea-ice expansion in CESM2. Conversely, pertaining to dQ-SA-TA, in the South Atlantic as well as in the Southern Ocean in general the MLD is larger in CESM2 than in CESM1, which should decelerate the cooling and sea-ice response in CESM2. However, as seen in Figs. 8c and S15f, respectively, CESM2 cools quicker and expands the Antarctic sea ice faster than CESM1. This indicates that other factors such as a stronger cloud feedback (Fig. S19) triggered by the Q-flux-induced surface cooling facilitate the sea-ice expansion in CESM2. Note that the base-state Q-flux and MLD are equivalent in CESM2 and CESM2-Z22.

CESM1 and CESM2 are also different in terms of base-state climatological wind patterns: The subtropical easterlies are slightly stronger in CESM2 than in CESM1 (Fig. S8c). This may facilitate the larger westward expansion of the cooling and the accompanying negative CRF_{SW} in CESM2 (Fig. 9 and cf. Figs. S6 and S20).

Differences between the models also exist in terms of base-state sea-ice area (Fig. S21). Notably, the base-state Antarctic sea-ice area in CESM2-Z22 is about 30% smaller than in CESM1 and CESM2. This may explain the slower response of CESM2-Z22 compared to the other models in dQ-SA-TA: More sea ice needs to build up before the SST-cloud feedback loop described in Sect. 4.1, which accelerates the sea-ice expansion, is triggered. Thus, it takes longer for CESM2-Z22 to enter the Snowball Earth state than for CESM1 and CESM2. However, we confirm a weaker cloud effect in CESM2-Z22 than in CESM2 also in the absence of sea ice (Fig. S22).

Finally, the differences in cloud parametrisation cause differences in base-state cloud distribution (Fig. S23) as well as different cloud responses between the three models versions

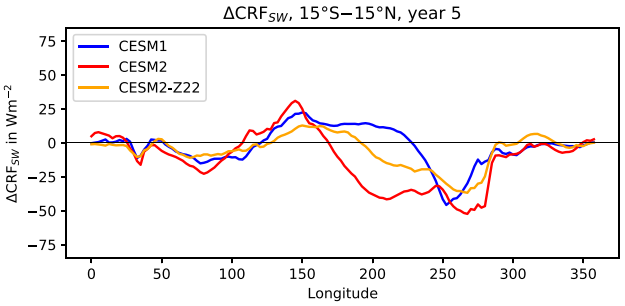

Fig. 9 Change of the short-wave cloud radiative flux (ΔCRF_{SW}) in the inner tropics (15° S-15° N) for (blue) CESM1, (red) CESM2, and (orange) CESM2-Z22 in year 5 of the respective dQ-EP-WP simulation

(Zhu et al. 2022). In the base state, CESM1 has the least cloud liquid water path (LWP). CESM2 exhibits much more LWP, with the CESM2-Z22 values being between the two other models. The difference between the models are concentrated mostly in the extra-tropics (>30°) over the oceans. The differences in cloud ice water path (IWP) between CESM2 and CESM2-Z22 are small, but both exhibit much less IWP than CESM1. While the LWP and IWP distributions are more realistic in CESM2 than in CESM1 (e.g., Gettelman et al. 2019; Bacmeister et al. 2020), according to Zhu et al. (2022), they are even more realistic in CESM2-Z22 than in CESM2. In response to dQ-EP-WP in the EP, the strongest LWP response is exhibited by CESM2, with a continuous increase throughout the simulation, while in CESM1 and CESM2-Z22 the LWP remains almost constant (Fig. 10a). The low-cloud cover response in the EP is similar to the LWP response (Fig. 10c). In the central Pacific both the LWP and the low-cloud cover almost instantly more than double in CESM2, while there is only a slight and slow increase in CESM2-Z22 and little response in CESM1 (Fig. 10b, d). The effect of low liquid clouds on CRF_{SW} was explained in Sect. 4.1 and the changes discussed here are consistent with Fig. 9. As mentioned above, the differences between CESM1 and CESM2 may be impacted by different MLD and base-state Q-fluxes, explaining part of the difference of the cloud response. However, there is no difference in these quantities between CESM2 and CESM2-Z22, indicating that the different cloud response is mostly due to the difference in cloud parametrisation. The main changes in the cloud microphysics parametrisation undertaken by Zhu et al. (2022) for CESM2-Z22 are the removal of the cloud ice number concentration delimiter and a substepping of the microphysics scheme, i.e., a shorter time-step. The change of the ice delimiter should mainly impact the ice clouds. However, in dQ-EP-WP in the EP and the central Pacific there is very little difference between CESM2 and CESM2-Z22 in terms of IWP (Fig. 10a, b), suggesting that this change

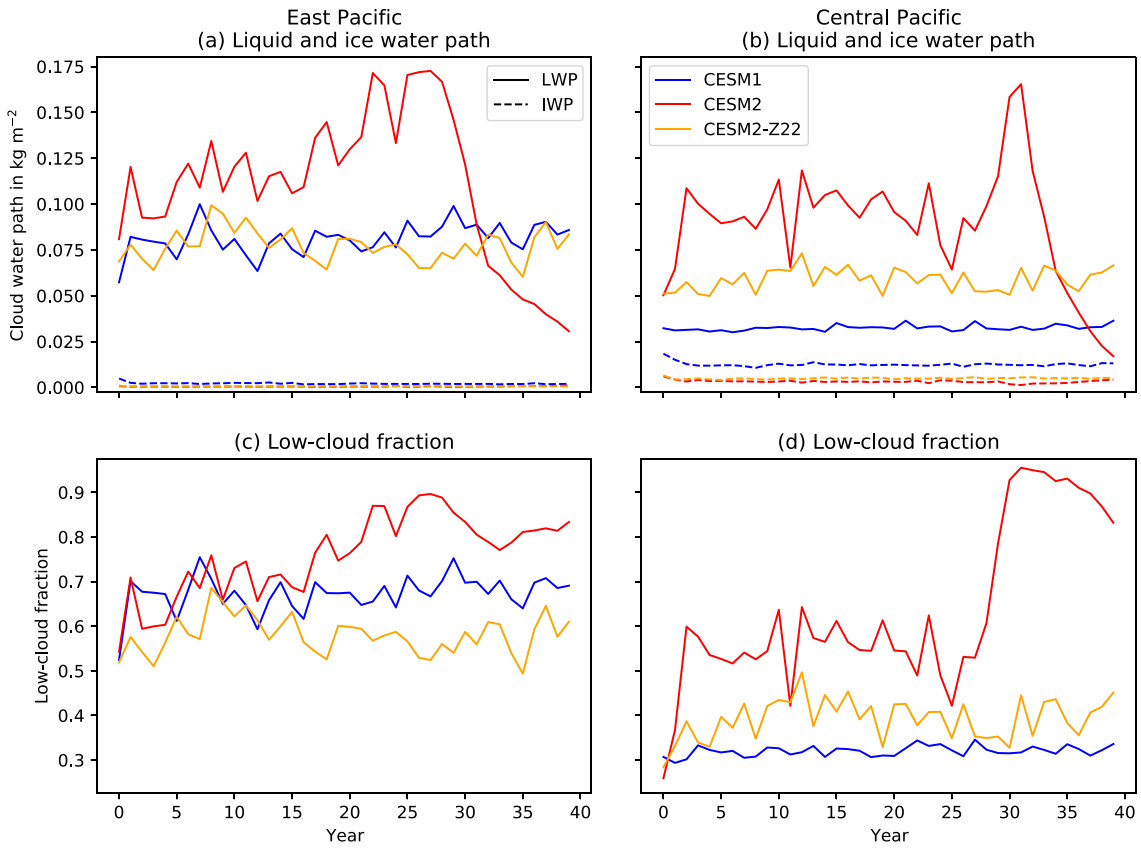

Fig. 10 Annual means of **a** East Pacific and **b** central Pacific cloud (solid) liquid and (dashed) ice water path (LWP and IWP, respectively), as well as **c** East Pacific and **d** central Pacific low-cloud fraction for (blue) CESM1, (red) CESM2, and (orange) CESM2-Z22 in dQ-EP-WP

to the cloud microphysics is not the cause for the difference between the models. Indeed, Zhu et al. (2022) find that the substepping of the microphysics scheme weakens the cloud feedback in their simulations of the LGM climate. However, the reasons for this are unclear. Zhu et al. (2022) mention that substepping has been found to affect rain evaporation and self-collection processes but no definitive conclusions are given. While we cannot give any definitive conclusions either, we report that in the East and central Pacific the precipitation in dQ-EP-WP declines more strongly in CESM2 than in CESM2-Z22 (Fig. S24), indicating that less precipitation leads to more LWP observed in CESM2 than in CESM2-Z22, inducing the stronger CRF_{SW}.

5 Conclusion

In this study we investigate the impact on the climate of a redistribution of energy across the Earth's surface. The investigation is motivated by the historically observed changes in surface-warming/cooling patterns and the idea of the pattern effect, i.e., that the patterns of surface warming affect the global-mean warming itself. Experiments are performed with a slab-ocean model with changed ocean heat transport convergence (Q-flux) to qualitatively mimic surface-warming changes. The impact on the global-mean surface temperature as well as individual radiative feedbacks in the climate system is investigated.

Even though the positive and negative Q-flux changes cancel perfectly by construction, all experiments exhibit a global cooling. This "asymmetry" in the response to positive and negative Q-flux changes is consistent with the findings of Liu et al. (2020). They attribute the asymmetry mostly to the effect of sea ice. However, here we also find an asymmetry, albeit much weaker, in the absence of sea ice, which is mainly due to the cloud feedback (Fig. S25). Liu et al. (2020) use CESM1 while our simulations with deactivated sea ice are performed with CESM2. Since these models differ significantly in the cloud response to Q-flux changes (Sect. 4.3) this may explain the different results.

We find another asymmetry between cooling in the Northern and Southern Hemispheres, similar to the results of Lin et al. (2021): A cooling in the North Atlantic, such as may be induced by a decline in the Atlantic meridional overturning circulation (AMOC; e.g., Eiselt and Graversen 2023), gives rise to a much weaker global cooling than a

similar local cooling in the South Atlantic. This is related to a geographically less constrained sea-ice development in the Southern Ocean than in the Arctic, as well as a strong feedback loop between the Southern Ocean and the stably stratified regions of the tropics (especially the East Pacific): Cooling in the Southern Ocean is advected via climatological winds into the stably stratified regions of the tropics, decreasing local sea-surface temperatures and increasing stability, causing enhanced cloud feedback due to increased low-cloud formation (Dong et al. 2022). More low clouds lead to more reflection of sunlight, inducing further local cooling, which in turn induces more low-cloud formation (Hwang et al. 2017; Kim et al. 2022; Kang et al. 2023).

Since in addition to the global-mean warming a CO_2-forcing may induce changes in surface-warming *patterns* (Eiselt and Graversen 2023; Seager et al. 2019; Lee et al. 2022), the linearity of the combined response to the Q-flux changes and CO_2-forcing is tested. We find that strong non-linearities are introduced by the sea-ice expansion and the accompanying surface-albedo feedback. In an experiment with deactivated sea ice, non-linearities are much smaller but non-negligible. In the absence of sea ice, the remaining non-linearities are introduced mainly by the cloud feedback, especially over the Southern Ocean and the East Pacific.

The dependence of the effects of the Q-flux changes on the specific employed climate model are investigated by comparing different versions of the same model, differing mainly in terms of cloud parametrisation. A significant dependence on these differences of the response to different Q-flux changes is found. This implies that the pattern effect in different climate models depends in particular on the cloud parametrisation, potentially associated with clouds being the largest contributor to differences between climate models in terms of the response to CO_2-forcing (Zelinka et al. 2020).

Finally, we caution against over-interpretation of our results. In an additional experiment, where a surface cooling of 10 Wm^{-2} is implemented over the whole Southern Ocean with a compensating surface warming in the tropics in the fully-coupled version of CESM2 by changing long-wave surface fluxes, the global-mean surface-air temperature decreases by only ~1 K after 70 years of simulation (Fig. 11). However, in such experiments with a full dynamical ocean, the ocean can react and set up a compensating circulation. Hence, it is thought-provoking, that a transition to a Snowball Earth is induced by comparatively small redistributions of surface energy in slab-ocean models, where by construction a compensating dynamical ocean circulation change cannot occur.

Supplementary Information The online version contains supplementary material available at https://doi.org/10.1007/s00382-024-07117-1.

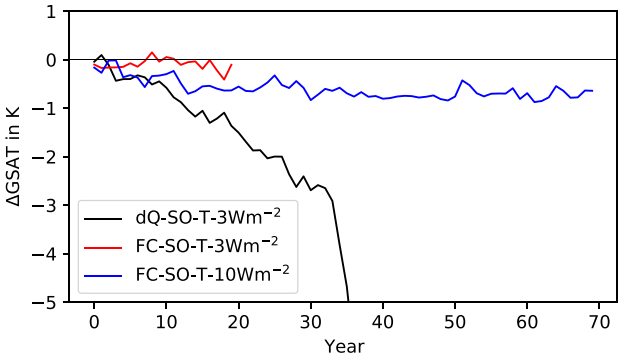

Fig. 11 Global-mean surface-air temperature change (ΔGSAT) in (black) dQ-SO-T-3Wm^{-2}, (red) FC-SO-T-3Wm^{-2}, and (blue) FC-SO-T-10Wm^{-2}. "FC" indicates the fully-coupled version of CESM2

Acknowledgements We thank two anonymous reviewers for their helpful suggestions.

Author Contributions K-UE and RGG conceived and designed the study. Material preparation, data collection and analysis were performed by K-UE. The first draft of the manuscript was written by K-UE with comments and revisions from RGG.

Funding Open access funding provided by UiT The Arctic University of Norway (incl University Hospital of North Norway). The data generated during this research is stored at the Nird storage facilities provided by the Norwegian e-infrastructure for research and education, UNINETT Sigma2, under the project NS9063K. The CESM simulations were performed on the FRAM supercomputer at the University of Tromsø (UiT) provided by UNINETT Sigma2, under the project NN9348k. The work is part of the project*UiT – Climate Initiative, Ice-ocean–atmosphere interactions in the Arctic – from the past to the future, funded by the Faculty of Science and Technology, University of Tromsø.*

Data Availability The proprietary CESM numerical model simulations presented in this study are too large to archive or to transfer. Instead, we provide all the information needed to replicate the CESM simulations (see Code availability); we used model versions 1.2.2 and 2.1.3, freely available at https://www2.cesm.ucar.edu/models/cesm1.2/ and https://www.cesm.ucar.edu/models/cesm2, respectively.

Code availability The code adjustments for CESM2-Z22 are available at https://doi.org/10.5065/bdr7-wt42. Pre- and postprocessing code for the CESM data are available at zenodo (https://doi.org/10.5281/zenodo.7950682), as are the scripts for changing the CESM code to run the experiments presented here (https://doi.org/10.5281/zenodo.8334523).

Declarations

Conflict of interest The authors have no relevant financial or non-financial interests to disclose.

Ethics approval Not applicable.

Consent to participate Not applicable.

Consent for publication Not applicable.

References

Andrews T, Webb MJ (2018) The dependence of global cloud and lapse rate feedback on the spatial structure of tropical Pacific warming. J Clim 31:641–654. https://doi.org/10.1175/JCLI-D-17-0087.1

Andrews T, Gregory JM, Webb MJ (2015) The dependence of radiative forcing and feedback on evolving patterns of surface temperature change in climate models. J Clim 28:1630–1648. https://doi.org/10.1175/JCLI-D-14-00545.1

Andrews T, Gregory JM, Webb MJ, Taylor KE (2012) Forcing, feedbacks and climate sensitivity in CMIP5 coupled atmosphere-ocean climate models. Geophys Res Lett 39. https://doi.org/10.1029/2012GL051607

Bacmeister JT, Hannay C, Medeiros B, Gettelman A, Neale R, Fredriksen HB, Lipscomb WH, Simpson I, Bailey DA, Holland M, Lindsay K, Otto-Bliesner B (2020) CO_2 increase experiments using the CESM: Relationship to climate sensitivity and comparison of CESM1 to CESM2. J Adv Model Earth Syst 12. https://doi.org/10.1029/2020MS002120

Bellomo K, Angeloni M, Corti S, Hardenberg J (2021) Future climate change shaped by inter-model differences in Atlantic meridional overturning circulation response. Nat Commun 12. https://doi.org/10.1038/s41467-021-24015-w

Bitz CM, Shell KM, Gent PR, Bailey DA, Danabasoglu G, Armour KC, Holland MM, Kiehl JT (2012) Climate sensitivity of the community climate system model, Version 4. J Clim 25:3053–3070. https://doi.org/10.1175/JCLI-D-11-00290.1

Bjordal J, Storelvmo T, Alterskjær K, Karlsen T (2020) Equilibrium climate sensitivity above 5° C plausible due to state-dependent cloud feedback. Nat Geosci 13:718–721. https://doi.org/10.1038/s41561-020-00649-1

Block K, Mauritsen T (2013) Forcing and feedback in the MPI-ESM-LR coupled model under abruptly quadrupled CO_2. J Adv Model Earth Syst 5:676–691. https://doi.org/10.1002/jame.20041

Boer GJ, Yu B (2003) Climate sensitivity and climate state. Clim Dyn 21.https://doi.org/10.1007/s00382-003-0323-7

Ceppi P, Gregory JM (2017) Relationship of tropospheric stability to climate sensitvity and Earth's observed radiation budget. Proc Natl Acad Sci (USA) 114:13126–13131. https://doi.org/10.1073/pnas.1714308114

Clement AM, Seager R, Cane MA, Zebiak SE (1996) An ocean dynamical thermostat. J Clim 9:2190–2196. https://doi.org/10.1175/1520-0442(1996)009<2190:AODT>2.0.CO;2

Danabasoglu G, Lamarque J-F, Bacmeister J, Bailey D-A, DuVivier A-K, Edwards J, Emmons L-K, Fasullo J, Garcia R, Gettelman A, Hannay C, Holland M-M, Large W-G, Lauritzen P-H, Lawrence D-M, Lenaerts J-T-M, Lindsay K, Lipscomb W-H, Mills M-J, Neale R, Oleson K-W, Otto-Bliesner B, Phillips A-S, Sacks W, Tilmes S, Kampenhout L, Vertenstein M, Bertini A, Dennis J, Deser C, Fischer C, Fox-Kemper B, Kay J-E, Kinnison D, Kushner P-J, Larson V-E, Long M-C, Mickelson S, Moore J-K, Nienhouse E, Polvani L, Strand P-JRW-G (2020) The Community Earth System Model Version 2 (CESM2). J Adv Model Earth Syst 12. https://doi.org/10.1029/2019MS001916

Dong Y, Proistosescu C, Armour KC, Battisti DS (2019) Attributing historical and future evolution of radiative feedbacks to regional warming patterns using a Green's function approach: The preeminence of the Western Pacific. J Clim 32:5471–5491. https://doi.org/10.1175/JCLI-D-18-0843.1

Dong Y, Armour KC, Zelinka MD, Proistosescu C, Battisti DS, Zhou C, Andrews T (2020) Intermodel spread in the pattern effect and its contribution of climate sensitivity in CMIP5 and CMIP6 models. J Clim 33:7755–7775. https://doi.org/10.1175/JCLI-D-19-1011.1

Dong Y, Armour KC, Battisti DS, Blanchard-Wrigglesworth E (2022) Two-way teleconnections between the Southern Ocean and the tropical Pacific via a dynamic feedback. J Clim 35:2667–2682. https://doi.org/10.1175/JCLI-D-22-0080.1

Dong Y, Pauling AG, Sadai S, Armour KC (2022) Antarctic ice-sheet meltwater reduces transient warming and climate sensitivity through the sea-surface temperature pattern effect. Geophys Res Lett 49. https://doi.org/10.1029/2022GL101249

Eiselt K-U, Graversen RG (2022) Change in climate sensitivity and its dependence on lapse-rate feedback in 4×CO_2 climate mode experiments. J Clim 35:2919–2932. https://doi.org/10.1175/JCLI-D-21-0623.1

Eiselt K-U, Graversen RG (2023) On the control of Northern Hemispheric feedbacks by AMOC: evidence from CMIP and slab ocean modeling. J Clim 36:6777–6795. https://doi.org/10.1175/JCLI-D-22-0884.1

Eyring V, Bony S, Meehl GA, Senior CA, Stevens B, Stouffer RJ, Taylor KE (2016) Overview of the Coupled Model Intercomparison Project Phase 6 (CMIP6) experimental design and organization. Geosci Model Dev 9:1937–1958. https://doi.org/10.5194/gmd-9-1937-2016

Gettelman A, Hannay C, Bacmeister JT, Neale RB, Pendergrass AG, Danabasoglu G, Lamarque J-F, Fasullo JT, Bailey DA, Lawrence DM, Mills MJ (2019) High climate sensitivity in the Community Earth System Model version 2 (CESM2). Geophys Res Lett 46:8329–8337. https://doi.org/10.1029/2019GL083978

Gregory JM, Ingram WJ, Palmer MA, Jones GS, Stott PA, Thorpe RB, Lowe JA, Johns TC, Williams KD (2004) A new method for diagnosing radiative forcing and climate sensitivity. Geophys Res Lett 31. https://doi.org/10.1029/2003GL018747

He J, Winton M, Vecchi G, Jia L, Rugenstein M (2017) Transient climate sensitivity depends on base climate ocean circulation. J Clim 30:1493–1504. https://doi.org/10.1175/JCLI-D-16-0581.1

Huguenin MF, Holmes RM, England MH (2022) Drivers and distribution of global ocean heat uptake over the last half century. Nat Commun 13. https://doi.org/10.1038/s41467-022-32540-5

Hurrell JW, Holland MM, Gent PR, Ghan S, Kay JE, Kushner PJ, Lamarque J-F, Large WG, Lawrence D, Lindsay K, Lipscomb WH, Long MC, Mahowald N, Marsh DR, Neale RB, Rasch P, Vavrus S, Vertenstein M, Bader D, Collins WD, Hack JJ, Kiehl J, Marshall S (2013) The Community Earth System Model: A framework for collaborative research. Bull Am Meteorol Soc 94:1339–1360. https://doi.org/10.1175/BAMS-D-12-00121.1

Hwang Y-T, Xie S-P, Deser C, Kang SM (2017) Connecting tropical climate change with Southern Ocean heat uptake. Geophys Res Lett 44:9449–9457. https://doi.org/10.1002/2017GL074972

Kang SM, Yu Y, Deser C, Zhang X, Kang I-S, Lee S-S, Rodgers KB, Ceppi P (2023) Subtropical clouds key to Southern Ocean teleconnections to the tropical Pacific. Proc Natl Acad Sci (USA) 120. https://doi.org/10.1073/pnas.2300881120

Kang SM, Xie S-P (2014) Dependence of climate response on meridional structure of external thermal forcing. J Clim 27:5593–5600. https://doi.org/10.1175/JCLI-D-13-00622.1

Kim H, Kang SM, Kay JE, Xie S-P (2022) Subtropical clouds key to Southern Ocean teleconnections to the tropical Pacific. Proc Natl Acad Sci (USA) 119. https://doi.org/10.1073/pnas.2200514119

Klein SA, Hartmann DL (1993) The seasonal cycle of low stratiform clouds. J Clim 6:1587–1606. https://doi.org/10.1175/1520-0442(1993)006<1587:TSCOLS>2.0.CO;2

Klein SA, Hall A, Norris JR, Pinus R (2017) Low-cloud feedbacks from cloud-controlling factors: a review. Surv Geophys 38:1307–1329. https://doi.org/10.1007/s10712-017-9433-3

Lee S, L'Heureux M, Wittenberg AT, Seager RNC, Johnson PAO (2022) On the future zonal contrasts of equatorial Pacific climate: Perspectives from observations, simulations, and theories. npj Clim Atmos Sci 5. https://doi.org/10.1038/s41612-022-00301-2

Lin Y-J, Hwang Y-T, Lu J, Liu F, Rose BEJ (2021) The dominant contribution of Southern Ocean heat uptake to time-evolving radiative feedback in CESM. Geophys Res Lett 48. https://doi.org/10.1029/2021GL093302

Lin Y-J, Hwang Y-T, Ceppi P, Gregory JM (2019) Uncertainty in the evolution of climate feedback traced to strength of the Atlantic meridional overturning circulation. Geophys Res Lett 46:12331–12339. https://doi.org/10.1029/2019GL083084

Lindzen R, Choi Y-S (2021) The iris effect: a review. Asia-Pac J Atmos Sci 58:159–168. https://doi.org/10.1007/s13143-021-00238-1

Liu F, Lu J, Garuba O, Leung LR, Luo Y, Wan X (2018) Sensitivity of surface temperature to oceanic forcing via q-flux Green's function experiments. Part I: Linear response function. J Clim 31:3625–3641. https://doi.org/10.1175/JCLI-D-17-0462.1

Liu F, Lu J, Garuba O, Leung LR, Harrop BE, Luo Y (2018) Sensitivity of surface temperature to oceanic forcing via q-flux Green's function experiments. Part II: Feedback decomposition and Polar Amplification. J Clim 31:6745–6761. https://doi.org/10.1175/JCLI-D-18-0042.1

Liu F, Lu J, Garuba O, Leung LR, Harrop BE, Luo Y (2020) Sensitivity of surface temperature to oceanic forcing via q-flux Green's function experiments. Part III: asymmetric response to warming and cooling. J Clim 33:1283–1297. https://doi.org/10.1175/JCLI-D-19-0131.1

Luo Y, Lu J, Liu F, Garuba O (2017) The role of ocean dynamical thermostat in delaying the El Niño-like response over the equatorial pacific to climate warming. J Clim 30:2811–2827. https://doi.org/10.1175/JCLI-D-16-0454.1

Manabe S, Wetherald WT (1975) The effects of doubling of the CO_2 concentration on the climate of a general circulation model. J Atmos Sci 32:3–15. https://doi.org/10.1175/1520-0469(1975)032<0003:TEODTC>2.0.CO;2

Mauritsen T (2016) Clouds cooled the earth. Nat Geosci 9:865–867. https://doi.org/10.1038/ngeo2838

Mauritsen T, Stevens B (2015) Missing iris effect as a possible cause of muted hydrological change and high climate sensitivity in models. Nat Geosci 8:346–351. https://doi.org/10.1038/NGEO2414

Mitevski I, Dong Y, Polvani LM, Rugenstein M, Orbe C (2023) Nonmonotonic feedback dependence under abrupt CO_2 forcing due to a North Atlantic pattern effect. Geophys Res Lett 50. https://doi.org/10.1029/2023GL103617

Murphy, J.M.: Transient response of the Hadley Centre coupled ocean-atmosphere model to increasing carbon dioxide. Part III: analysis of global-mean response using simple models. J Clim 8:496–514 (1995) https://doi.org/10.1175/1520-0442(1995)008<0496:TROTHC>2.0.CO;2

Po-Chedley S, Armour KC, Bitz CM, Zelinka MD, Santer BD, Fu Q (2018) Sources of intermodel spread in the lapse rate and water vapor feedbacks. J Clim 31:3187–3206. https://doi.org/10.1175/JCLI-D-17-0674.1

Rose BEJ, Armour KC, Battisti DS, Feldl N, Koll DDB (2014) The dependence of transient climate sensitivity and radiative feedbacks on the spatial pattern of ocean heat uptake. Geophys Res Lett 41:1071–1078. https://doi.org/10.1002/2013GL058955

Rugenstein MAA, Caldeira K, Knutti R (2016) Dependence of global radiative feedbacks on evolving patterns of surface heat fluxes. Geophys Res Lett 43:9877–9885. https://doi.org/10.1002/2016GL070907

Seager R, Cane M, Henderson N, Lee D-E, Abernathy R, Zhang H (2019) Strengthening tropical Pacific zonal sea surface temperature gradient consistent with rising greenhouse gases. Nat Clim Change 9:517–525. https://doi.org/10.1038/s41558-019-0505-x

Senior CA, Mitchell JFB (2000) The time-dependence of climate sensitivity. Geophys Res Lett 27:2685–2688. https://doi.org/10.1029/2000GL011373

Shell KM, Kiehl JT, Shields CA (2008) Using the radiative kernel technique to calculate climate feedbacks in NCAR's Community Atmospheric Model. J Clim 21:2269–2282. https://doi.org/10.1175/2007JCLI2044.1

Singh H, Feldl N, Kay JE, Morrison AL (2022) Climate sensitivity is sensitive to changes in ocean heat transport. J Clim 35:2653–2674. https://doi.org/10.1175/JCLI-D-21-0674.1

Soden BJ, Held IM, Colman R, Shell KM, Kiehl JT, Shields CA (2008) Quantifying climate feedbacks using radiative kernels. J Clim 21:3504–3520. https://doi.org/10.1175/2007JCLI2110.1

Stephens GL (1978) Radiation profiles in extended water clouds. II: Parameterization schemes. J Atmos Sci 35: 2123–2132. https://doi.org/10.1175/1520-0469(1978)035<2123:RPIEWC>2.0.CO;2

Stevens B, Sherwood SC, Bony S, Webb MJ (2016) Prospects for narrowing bounds on Earth's climate sensitivity. Earth's Future 4:512–522. https://doi.org/10.1002/2016EF000376

Taylor KE, Stouffer RJ, Meehl GA (2009) A summary of the CMIP5 experiment design. Tech Rep. https://pcmdi.llnl.gov/mips/cmip5/docs/Taylor_CMIP5_design.pdf?id=98

Wallace JM, Hobbs PV (2006) Atmospheric Science: An Introductory Survey. Academic Press, 525 B Street, Suite 1900, San Diego, CA

Wills RCJ, Dong Y, Proistosecu C, Armour KC, Battisti DS (2022) Systematic climate model biases in the large-scale patterns of recent sea-surface temperature and sea-level pressure change. Geophys Res Lett 49. https://doi.org/10.1029/2022GL100011

Wood R, Bretherton CS (2006) On the relationship between stratiform low cloud cover and lower-tropospheric stability. J Clim 19:6425–6432. https://doi.org/10.1175/JCLI3988.1

Xie S-P, Philander SGH (1994) A coupled ocean-atmosphere model of relevance to the ITCZ in the Eastern Pacific. Tellus A Dyn Meteorol Oceanogr 46:340–350. https://doi.org/10.3402/tellusa.v46i4.15484

Zelinka MD, Meyers TA, McCoy DT, Po-Chedley S, Caldwell PM, Ceppi P, Klein SA, Taylor KE (2020) Causes of higher climate sensitivity in CMIP6 models. Geophys Res Lett 47. https://doi.org/10.1029/2019GL085782

Zhang L, Delworth TL, Cooke W, Yang X (2019) Natural variability of Southern Ocean convection as a driver of observed climate trends. Nat Clim Change 9:59–65. https://doi.org/10.1038/s41558-018-0350-3

Zhou C, Zelinka MD, Klein SA (2016) Impact of decadal cloud variations on the Earth's energy budget. Nat Geosci 9:871–874. https://doi.org/10.1038/NGEO2828

Zhou C, Zelinka MD, Klein SA (2017) Analyzing the dependence of global cloud feedback on the spatial pattern of sea surface temperature change with a Green's function approach. J Adv Model Earth Syst 9:2174–2189. https://doi.org/10.1002/2017MS001096

Zhu J, Otto-Bliesner BL, Brady EC, Gettelman A, Bacmeister JT, Neale RB, Poulsen CJ, Shaw JK, McGraw ZS, Kay JE (2022) LGM paleoclimate constraints inform cloud parameterizations

and equilibrium climate sensitivity in CESM2. J Adv Model Earth Syst 14. https://doi.org/10.1029/2021MS002776

Zhu J, Otto-Bliesner BL, Brady EC, Poulsen CJ, Tierney JE, Lofverstrom M, DiNezio P (2021) Assessment of equilibrium climate sensitivity of the Community Earth System Model version 2 through simulation of the last glacial maximum. Geophys Res Lett 14. https://doi.org/10.1029/2020GL091220